Title

Maladaptive brain organization at 1 month into abstinence as an indicator for future relapse in patients with alcohol use disorder

Journal

European Journal of Neuroscience, 53(8)

ISSN

0953-816X

Authors

Muller, Angela M
Meyerhoff, Dieter J

Publication Date

2021-04-01

DOI

10.1111/ejn.15161

Peer reviewed

Received: 18 November 2020 | Revised: 22 February 2021 | Accepted: 23 February 2021

DOI: 10.1111/ejn.15161

RESEARCH REPORT

EJN European Journal of Neuroscience FENS WILEY

Maladaptive brain organization at 1 month into abstinence as an indicator for future relapse in patients with alcohol use disorder

Angela M. Muller | **Dieter J. Meyerhoff**

Department of Radiology and Biomedical Imaging, University of California San Francisco, San Francisco, CA, USA

Correspondence
Angela M. Muller, Department of Radiology and Biomedical Imaging, VA Advanced Imaging Research Center, San Francisco VA Medical Center, 4150 Clement Street, Building 13, San Francisco, CA, 94121, USA.
Email: angela.muller@ucsf.edu

Funding information
NIH, Grant/Award Number: AA010788 and DA039903; DoD, Grant/Award Number: W81XWH-15-2-0020

Abstract

Abstinence is a lifelong endeavor, and the risk of a relapse is always present for patients with Alcohol Use Disorder (AUD). The aim of the study was to better understand specific characteristics of the intrinsic whole-brain-network architecture of 34 AUD patients that may support abstinence or relapse. We used Graph Theory Analysis (GTA) of resting-state fMRI data from treatment seekers at 1 month of abstinence and their follow-up data as abstainers or relapsers 3 months later, together with data from 30 light/non-drinking controls scanned at the same interval. We determined the group-specific intrinsic community configurations at both timepoints as well as the corresponding modularity Q, a GTA measure that quantifies how well individual network communities are separated from each other. Both AUD groups at both timepoints had community configurations significantly different from those of controls, but the three groups did not significantly differ in their Q values. However, relapsers showed a maladaptive community configuration at baseline, which became more similar to the controls' community organization after the relapsers had started consuming alcohol again during the study interval. Additionally, successful recovery from AUD was not associated with re-gaining the intrinsic brain organization found in light/non-drinkers, but with a re-configuration resulting in a new brain organization distinctly different from that of healthy controls. Resting-state fMRI provides useful measures reflecting neuroplastic adaptations related to AUD treatment outcome.

KEYWORDS

brain reward system, default mode network, integration, participation coefficient, segregation, subnetwork

Abbreviations: ABS, abstainers; AICHA, Atlas of Intrinsic Connectivity of Homotopic Areas; ART, Artifact Detection Toolbox; AUD, alcohol use disorder; AUDIT, Alcohol Use Disorder Identification Test; BCT, Brain Connectivity Toolbox; BDI, Beck Depression Inventory; BIS-11, Barratt Impulsivity Scale; BOLD, Blood Oxygenation Level Dependent; CSF, cerebral spinal fluid; DAN, dorsal attention network; DMN, default mode network; dmPFC, dorsal medial prefrontal cortex; eBRS, extended brain reward system; ECN, executive control network; EPI, echo planar imaging; FA, flip angle; FOV, field of view; FTND, Fagerström Test for Nicotine Dependence; GIC, global integration coefficient; GTA, Graph Theory Analysis; ICN, intrinsic connectivity network; IQ, interquartile distance; LDC, light/non drinking controls; MRI, magnet resonance imaging; PACE, prospective acquisition correction; PC, participation coefficient; REL, relapsers; SA, salience network; SMN, sensorimotor network; STAI, State-Trait Anxiety Inventory; TE, echo time; TP1, baseline (= one month of abstinence); TP3, follow-up (= three months after baseline); TR, repetition time; TSE, turbo spin echo; VIS, visual network.

Edited by: John Foxe

1 | INTRODUCTION

About 40%–60% of all patients with alcohol use disorder (AUD) undergoing treatment will relapse within the first year (Kirshenbaum et al., 2009). Such a high relapse rate makes it desirable to have a biomarker that identifies patients with elevated risk for relapse early in treatment. Abundant literature demonstrates that abstinence from alcohol is commonly associated with structural change and neurocognitive improvements (Meyerhoff & Durazzo, 2020). In substance-dependent patients gradual neuroplastic change may precede necessary behavioral changes to maintain abstinence and resist relapse (Brooks et al., 2020). Consequently, we hypothesized that those AUD patients whose brains demonstrate greater plastic changes during and after treatment are also more successful in escaping the often-lifelong cycle of excessive drinking, withdrawal, abstinence, and relapse than those with less prominent neuroplastic changes.

Brain modularity Q, a metric that quantifies the subnetwork organization of the brain, was recently suggested as a "biomarker of plasticity" to explain differential gain in cognitive function after cognitive training or aerobic exercise (Gallen & D'Esposito, 2019). Modularity (Girvan & Newman, 2002) is a concept from the mathematical branch of graph theory analysis (GTA), which uses two elements, nodes and edges between the nodes, to describe and understand complex networks. Modularity describes to which extent a network can be partitioned into distinct non-overlapping subnetworks or "communities" that are characterized by a maximal number of within-community edges and a minimal number of between-community edges (Rubinov & Sporns, 2010, 2011). In real-world networks, Q ranges from zero to one. The closer Q is to one, the higher is the network's modularity. Modularly organized networks have been shown to be highly efficient in regulating the information integration in the brain with minimum energy cost (Bullmore & Sporns, 2012). The potential modularity Q to predict positive plastic changes has already been shown in other populations than AUD patients. For example, patients with traumatic brain injury or healthy adults whose intrinsic brain organization at baseline was characterized by a high Q value showed the greatest cognitive improvement after undergoing cognitive training or aerobic exercise with presumed neuroplastic adaptations (Arnemann et al., 2015; Baniqued et al., ,,2018, 2019; Gallen et al., 2016).

Since modularity has successfully been used to differentiate between participants who will respond to training interventions and those who will not (Arnemann et al., 2015; Baniqued et al., ,2018, 2019; Gallen et al., 2016), we here investigated if modularity also helps to better understand why some patients benefit from AUD treatment, while others do not. Furthermore, a Q value always quantifies the modularity of a specific and unique community configuration. Community configurations differ from each other regarding brain regions/network nodes allocated to specific communities and/or regarding how nodes of the same community interact, or how different communities interact with each other. Therefore, we postulated that different community configurations in behaviorally different study groups can shed light on properties of community configurations that support successful treatment outcomes.

The specific study aim was to determine if the combination of group-specific Q values and their corresponding community configurations can differentiate early in treatment between AUD treatment seekers who will remain abstinent and will have relapsed at follow-up. Additionally, we wanted to understand better how the communities interact with each other and, how the regions of the extended brain reward system (eBRS; Durazzo et al., 2011; Makris et al., 2008) are distributed within the group-specific community configurations. The eBRS is critically involved in the development and maintenance of all forms of addictive disorders. For that purpose, we analyzed resting-state fMRI data from AUD patients obtained 1 month into treatment and 3 months later when they had either remained abstinent or had relapsed; we also compared their brain configurations to that of light/non-drinking controls.

2 | METHODS

2.1 | Participants

For the study presented here, we analyzed resting-state fMRI (rs-fMRI) data from a final sample of 34 AUD individuals of a larger group of substance abuse patients recruited from outpatient treatment clinics at the San Francisco Veterans Administration Medical Center Substance Abuse Day Hospital and the Kaiser Permanente Chemical Dependence Recovery. All 34 underwent our MRI protocol at approximately 1 month of abstinence (baseline), while still in outpatient treatment, and 24 returned for a follow-up scan after approximately 3 months (follow-up). The drinking status of the AUD patients at follow-up, ascertained by an in-person interview, determined their group membership for this analysis: 12 AUD individuals (10 of them returning for the 3-month follow-up) had stayed sober and were classified as abstainers, whereas 22 AUD individuals (14 of them returning for follow-up) had started consuming alcohol again during the 3-months interval and were classified as relapsers. Relapsers were asked to refrain from alcohol consumption the day and evening before their follow-up scan, which usually occurred in the late afternoon. We also analyzed the rs-fMRI data of 30 control participants from the local community, 21 of whom came back for a follow-up. All study participants had to have a breath alcohol concentration of zero at the time of scanning.

Basic demographics are summarized by group and timepoint in Table 1.

The screening section of the Structural Clinical Interview for DSM-5 Axis I disorders was administered to all participants. All AUD individuals had moderate or severe AUD and no other moderate or severe substance use disorder. Exclusion criteria for all participants included a history of neurologic disorder, e.g., epilepsy, traumatic brain injury with loss of consciences > 30 min, cerebrovascular disease, a history of general medical diseases such as untreated hypertension, diabetes, hypo/hyperthyroidism, and psychiatric diseases such as major depression, anxiety, trauma, and PTSD. Additionally, to be included in the study presented here, enrolled study participants had to have at least 150 volumes of rs-fMRI data left after cleaning the data from motion and physiological noise.

All participants underwent a battery of interviews and standardized questionnaires that included the Beck Depression Inventory (BDI, Beck et al., 1961), Barratt Impulsivity Scale (BIS-11, Patton et al., 1995), and the State-Trait Anxiety Inventory (STAI, Spielberger (1983), which uses 20 questions to assess the transient emotional status of a person when facing a stressful situation like an exam or a job interview (=state) and another 20 questions to assess a person's predisposition to react with anxiety in stressful situations (= trait). Alcohol use was measured using the Alcohol Use Disorder Identification Test (AUDIT, Saunders et al., 1993), which assesses with 10 questions potential hazardous alcohol use, potential alcohol dependence, and experience of alcohol harm. Tobacco use was measured using the Fagerström Test for Nicotine Dependence (FTND; Heatherton et al., 1991). The Committees on Human Research at the University of California San Francisco and the VA Medical Center had approved the study. Signed informed consent had been obtained from each participant prior to any research procedures in accordance with the Declaration of Helsinki.

2.2 | MRI data

The MRI data were collected at the VA Medical Center San Francisco on a 3.0 T MRI scanner (Siemens Magnetom Skyra Syngo MR D13) using a 20 channel receive head coil. The study used (a) a T1 weighted MPRAGE sequence with repetition time (TR) = 2,300 ms, echo time (TE) = 2.98 ms, flip angle (FA) = 9^0, field of view (FOV) = $256 \times 256 \times 192$ mm^3, isotropic voxel size $1 \times 1 \times 1$ mm^3, 192 transverse slices per volume, acquisition duration = 5.28 min; (b) a T2 weighted TSE sequence with TR = 9,000 ms, TE = 91 ms, FA = 150^0, FOV = $230 \times 230 \times 162$ mm^3, voxel size $0.9 \times 0.9 \times 3$ mm^3, 35 axial slices per volume, acquisition duration = 2.44 min; and (c) a whole brain task-free echo planar imaging (EPI) blood oxygen level-dependent ep2d PACE sequence with TR = 2020 ms,

TABLE 1 Demographic description of the three groups: Controls (LDC), abstainers (ABS), relapsers (REL)

	TP1			TP2		
	LDC	ABS	REL	LDC	ABS	REL
N	30	12	22	21	10	14
Age [years]	44.2 (11.1)	37.1 (7.8)	43.9 (10.4)	42.6 (10.9)	38.1 (8.5)	43.2 (9.2)
Gender F|M [*n*|	12|18	8|4	8|14	7|14	6|4	5|9
Education [years]	15.9 (2.4)	14.7 (1.9)	14.8 (2.0)	16.1 (2.5)	14.7 (1.6)	15.6 (1.6)
AUDIT	1.78 (1.37)	33.18 (5.19)**	30.67 (5.13)**	—	—	—
1-year average [drinks/month]	6.1 (8.3)	367.0 (206.1)**	355.2 (243.8)**	7.5 (9.9)	329.6 (192.9)*	384.8 (297.4)**
Lifetime average [drinks/month]	8.7 (7.3)	183.9 (93.6)**	190.4 (98.6)**	7.9 (6.8)	160.9 (80.7)**	197.6 (111.8)*
Smokers No/Current/Former [*n*]	15|3|4	7|2|3	10|9|3	8|3|2	6|2|2	7|4|3
FTND Total score	2.1 (2.0)	1.6 (2.3)	2.7 (2.1)	2.0 (1.8)	1.3 (1.5)	2.3 (2.2)
BIS-II-Total score	55.1 (9.9)	65.8 (8.8) *	66.6 (11.7)**	54.4 (10.9)	62.3 (11.6)	63.1 (9.3) *
BDI Total score	3.1 (3.9)	12.0 (8.9)**	15.0 (7.5)**	2.6 (2.8)	7. (6.8)	9.9 (5.8)**
STAI State score	23.9 (5.4)	37.5 (11.0)*	38.2 (12.6)**	25.3 (8.8)	35.7 (12.0)*	33.5 (9.6)
STAI Trait score	30.9 (8.9)	47.0 (11.7)**	47.5 (11.5)**	30.1 (6.8)	41.9 (10.6)*	38.8 (10.5)*

Note: Mean value with standard deviation in brackets; one asterisk = $p < .05$, two asterisks = $p < .001$ indicate the statistical level on which a group differed from the controls. The controls were pooled from three contemporaneously performed research studies, so not all demographic variables were consistently available. The variables other than age, gender, and education were obtained from 22 controls at baseline and 9 controls at follow-up.

Abbreviations: AUDIT, Alcohol Use Disorder Identification Test; BDI, Beck Depression Inventory; BIS-II, Barratt Impulsiveness Scale; FTND, Fagerstrom Test for Nicotine Dependence; STAI State/STAI Trait, State-Trait Anxiety Inventory; TP, timepoint.

TE = 27 ms, FA = 77^0, FOV = 220 × 220 × 129.5 mm^3; voxel size 2.5 × 2.5 × 3.5 mm^3, 37 axial slices per volume, acquisition duration = 8.08 min, 240 volumes.

2.3 | Pre-processing of the MRI data

SPM12 (https://www.fil.ion.ucl.ac.uk/spm/) running on MATLAB 2018b (Natick, Massachusetts: The MathWorks Inc.) was used for all pre-processing steps of the functional and structural MRI data. (a) The first ten volumes of the EPI data were removed to minimize T1 saturation effects, leaving 230 volumes for analysis. (b) The EPI data were slice time-corrected for descending acquisition and aligned to a mean EPI image by a two-step procedure. Only the motion-parameter file and the mean image of that first alignment step were used for the further pre-processing steps. (c) The T2 weighted image was co-registered to the T1 weighted image and the mean EPI image co-registered to the T2 weighted image. (d) A second alignment step was performed by which the original 230 EPI volumes were co-registered to the mean-EPI image from the first alignment. (e) The T1 weighted image was segmented into the three brain tissue maps using the "New Segmentation" algorithm of SPM12. (f) A study population-specific template was created using the DARTEL procedure (Ashburner, 2007) to be used for the normalization step, in which the structural and functional images were normalized to the MNI-space. During this step, both image types were resampled to a $2mm^3$ voxel size and only minimally smoothed using an isotropic Gaussian kernel (FWHM 1mm) in order to minimize possible spurious correlations for the following graph theoretical analyses.

2.4 | Denoising of the RS-FMRI data and computing correlation matrices

Denoising of the rs-fMRI data and computing subject-specific Pearson correlation matrices were performed using Conn (Version18b; https://www.nitrc.org/projects/conn/) running on MATLAB (MATLAB 2018b). The aCompCor method (Behzadi et al., 2007) was used to detect low-frequency physiological confounding signals like breathing or heartbeat by extracting the Blood Oxygenation Level-Dependent (BOLD) signal from the subject-specific white matter and cerebrospinal fluid (CSF) masks (five principal components each). The Artifact Detection Toolbox (ART) was used to identify motion corrupted outliers (global-signal z value threshold 5; subject-motion threshold 0.9 mm), volumes identified as outliers were censored by dummy-coding them as nuisance regressors for the subsequent regression. In a final step, the identified movement outliers, the physiological confounds, and the realignment parameters (12 regressors: 6 motion parameters and 6 first-order temporal derivatives) were regressed out. The data were band-pass filtered (0.008–0.09 Hz), detrended (linear, quadratic, and cubic), and despiked. We used Student *t* tests with the *composite motion measure* implemented in ART and the number of volumes identified as outliers by the denoising procedure as dependent variables to assess that the three groups did not significantly differ in motion artifacts and confounding signals.

2.5 | Network generation

To define the nodes for our GTA, we used the Atlas of Intrinsic Connectivity of Homotopic Areas (AICHA, Joliot et al., 2015) to partition the brain into 384 regions of interest (ROIs). Both positive and negative BOLD-signal correlations were used to compute unthresholded, positively, and negatively weighted edges between the 384 ROIs. Thresholding has the purpose to create a sparse network with only the strongest edges and to eliminate weaker edges with a higher probability of being spurious. However, we decided against thresholding the edges for the following reasons: (a) Thresholding the edge weights in clinical populations can induce spurious group differences (van den Heuvel et al., (2017); Hallquist and Hillary, (2018)). (b) Weak edges can be physiologically important (Santarnecchi et al., 2014) and the most dynamic connections, to which connections between communities likely belong (Zalesky et al., (2014), have correlations coefficients near zero.

2.6 | Defining the extended brain reward system (eBRS) using AICHA rois

To investigate how the eBRS is integrated within the brain's intrinsic communities, we defined the ROIs of the AICHA partition that corresponds best to the regions of the eBRS as described earlier (Durazzo et al., 2011; Makris et al., 2008). We used 62 ROIs of the AICHA parcellation to build the following composites: Bilateral nucleus accumbens, anterior thalamus, amygdala, hippocampus, and parahippocampal gyrus, anterior insula, lateral orbital prefrontal cortex, dorsolateral prefrontal cortex, ventromedial prefrontal cortex, and temporal pole.

2.7 | Computation of the group- and timepoint-specific community structure and degree of community integration

Brain Connectivity Toolbox routines (BCT; Rubinov and Sporns, 2019) were used to compute the GTA measurements described below.

2.8 | First Step: Defining a group- and timepoint-specific community-configuration

To define consensus community configurations that are representative for each group and timepoint (Betzel & Bassett, 2017), we followed a similar procedure as described in Cohen & D'Esposito, 2016. Ten thousand iterations of the Louvain algorithm (Blondel et al., 2008; Rubinov & Sporns, 2010) were run with a resolution parameter $\gamma = 1.6$ and the subjects' individual connectivity matrices as input to determine community configuration for each group at each timepoint. Simultaneously, the Q value was computed for each iteration and a subject-specific agreement matrix, which coded how often two nodes were allocated to the same community over the 10,000 iterations. The resulting individual agreement matrices of the subjects were used to compute group- and timepoint-specific average agreement matrices. These were the input for the subsequent computation of a consensus partition (Lancichinetti & Fortunato, 2012). For the consensus partition, the Louvain algorithm was run with 10,000 iterations (Brain Connectivity Toolbox (BCT), Rubinov & Sporns, 2010) on the average agreement matrix of each group at each timepoint until the re-clustered agreement matrices converged into a single cluster solution (=consensus partition) for that group at that timepoint.

2.9 | Second step: Determining the degree of global between-community interaction of the communities

We computed the participation coefficient (PC, (Guimerà & Ameral, 2005) adapted for weighted unthresholded networks (Rubinov & Spoons, 2011), which measures the degree to which a node is involved in the global between-community information integration. A node with a PC value near 1 is characterized by a high number of between-community connections and qualifies as a connector hub that facilitates the between-community integration (Sporns & Betzel, 2016). When using connectivity matrices with positive and negative correlations, it is possible to compute a PC value for the negatively correlated edges of every individual node as well (Rubinov & Sporns, 2011). A node with a PC value near 1 for its negatively correlated edges is segregated or decoupled from the global between-community information integration.

The absolute "negative" PC value of each node was subtracted from its absolute "positive" PC value to generate a single value to describe a node's importance for the between-community communication. A positive result indicates that the node has predominantly an integrative role in the global between-community communication, a negative result means that the node is not participating in the global between-community communication. This combined PC metric is referred to as "global integration coefficient" (GIC) for the rest of the manuscript. To investigate how the communities interacted with each other, we computed the average GIC value of all nodes within a community.

2.10 | Statistics

Neither PC nor GIC was normally distributed, hence we used Wilcoxon Rank Sum tests for the group statistics. Non-parametric permutations as described in Bassett et al. (2008) were used to assess if differences in subnetwork configurations between relapsers/abstainers versus controls could have been happened just by chance or were a unique and significant feature of the respective AUD subgroup. For that purpose, we created the following pairs at each timepoint: "controls versus relapsers," "controls versus abstainers," "abstainers versus relapsers." The following steps were repeated for each of these pairs and timepoints separately. (a) The individually computed subject agreement matrices of the two groups were randomly re-allocated to one of the two groups in such a way that the original group size was kept. (b) A new average agreement matrix for each of the permutated groups was calculated and (c) used as input for all the steps described in the section *Defining a group- and timepoint-specific subnetwork-configuration*. The result was a new individual community configuration reflecting the community structure for each of the permutated groups. The steps a-c were repeated 5,000 times. We counted how often a specific community of the original group from a certain timepoint could also be found in the 5,000 permuted community configurations. That number was used to compute the p value (number of observations/number of permutations). Bonferroni corrections were used when appropriate.

3 | RESULTS

3.1 | Demographics

As expected, both AUD groups had higher measures of lifetime drinking severity than the controls (Table 1). Relapsers and abstainers scored higher on BIS-11 and BDI scores than the controls at baseline, but only relapsers still had higher BIS-11 and BDI scores than the controls at follow-up. Abstainers showed higher state and trait anxiety scores than controls at both timepoints; relapsers also revealed higher state and trait anxiety scores than controls at baseline, but only higher trait anxiety at follow-up.

AUD participants with 3-months follow-up differed from those who dropped out (Table S1). Participants with follow-up had more years of education at either timepoint than dropouts. Abstainers without follow-up also had greater

substance use severities than those returning for study: they had consumed more monthly alcoholic drinks over lifetime and had a higher score on the Fagerström Test for Nicotine Dependence (both $p = .039$).

3.2 | Motion

The three groups did not differ significantly in motion artifacts or other physiological confounds (Table S2).

4 | RESULTS OF THE GRAPH THEORY ANALYSES

4.1 | Description of the community configurations

At both timepoints, we found a three-community configuration for controls and relapsers. Abstainers also had a three-community configuration at baseline, but at follow-up, abstainers had a four-community configuration (Figure 1). Community 1 in the three-community configuration (Figure 1 = dark blue) covered the bilateral lateral and the medial superior frontal gyri, parts of the bilateral middle frontal gyrus extending into the lateral and medial orbitofrontal cortex, further covering the temporal pole, middle and inferior temporal gyrus with hippocampus and parahippocampal gyrus and extending into the angular gyrus and parts of the precuneus. On the brain's midline, community 1 covered the anterior and posterior cingulate gyri, as well as large sections of the thalamus and basal ganglia. The brain regions covered by community 1 correspond approximately to regions belonging to the default mode network (DMN) and the limbic network (Doucet et al., 2019).

Community 2 (Figure 1 = light green) included the most posterior parts of the superior and middle frontal gyri, the supplementary motor area, the sensorimotor cortex with the insular cortex, and the Rolandic operculum extending into the inferior parietal cortex and the middle cingulate cortex on the brain's midline. This community corresponds approximately to the regions of the executive control network (ECN), the dorsal attention network (DAN), the salience network (SN), and the sensorimotor network (SMN; Doucet et al., 2019).

Community 3 (Figure 1 = red) encompassed the visual network (VIS; Doucet et al., 2019).

The most salient feature of the abstainers' four-community configuration at follow-up was that a section of the DMN, the dorsal medial prefrontal cortex (dmPFC) subsystem (Andrews-Hanna et al., 2010) that consists of the dmPFC and the temporoparietal junction, had separated from the DMN and formed a new community (community 2a) together with regions corresponding to the DAN and SN (Figure 1). At follow-up, community 2 of the abstainers at baseline was reduced to the somatomotor regions only (now community 2b).

4.2 | Modularity—Q value

At both timepoints, abstainers presented with higher Q values (baseline 0.2459; follow-up 0.2438) than relapsers (baseline 0.2297; follow-up 0.2337) and controls (baseline 0.2296; follow-up 0.2399). Although relapsers had a minimally higher Q value than controls at baseline and a lower Q than controls at follow-up (Figure 2), none of the group differences reached statistical significance ($p \leq .05$).

4.3 | Similarity of the community configurations: Percent of shared network allocation and results of the permutation testing

Controls, relapsers, and abstainers shared the community allocation of 84%–91% of the nodes at baseline and of 65%–91% of the nodes at follow-up (Figures S1a-f). Permutation tests (Table 2) evaluated if the exact combination of nodes forming a specific community found in one group could also have been observed by chance in one of the other two groups. Although three of the relapsers' communities could also have been found by chance in one of the other two groups (for details see the three comparisons categorized as "ns" in Table 2), the permutation tests showed that the probability of observing the exact triple or quadruple combination of communities of one group in one of the other two had a close-to-zero statistical probability ($p < .002$) at both baseline and follow-up.

4.4 | Differences in the community configurations: Allocation of the basal ganglia and thalamus nodes at baseline and follow-up

Figure 3 and Figures S1a, S1c in the supplement illustrate that at baseline, the allocation of the basal ganglia and thalamus nodes to community 2 instead of community 1 was the aspect in which the relapsers' community configuration differed most prominently from those of abstainers and controls. In relapsers, 89% of the basal ganglia and thalamus nodes were allocated to community 2, whereas most of these nodes in controls and abstainers were allocated to community 1 (controls = 76%; abstainers = 87%). Permutation testing demonstrated that these node allocations to community 2 were significantly specific for relapsers. The probability to find that configuration by chance in controls was 0.16% ($p = .0016$) and 0.24% ($p = .0024$) in abstainers.

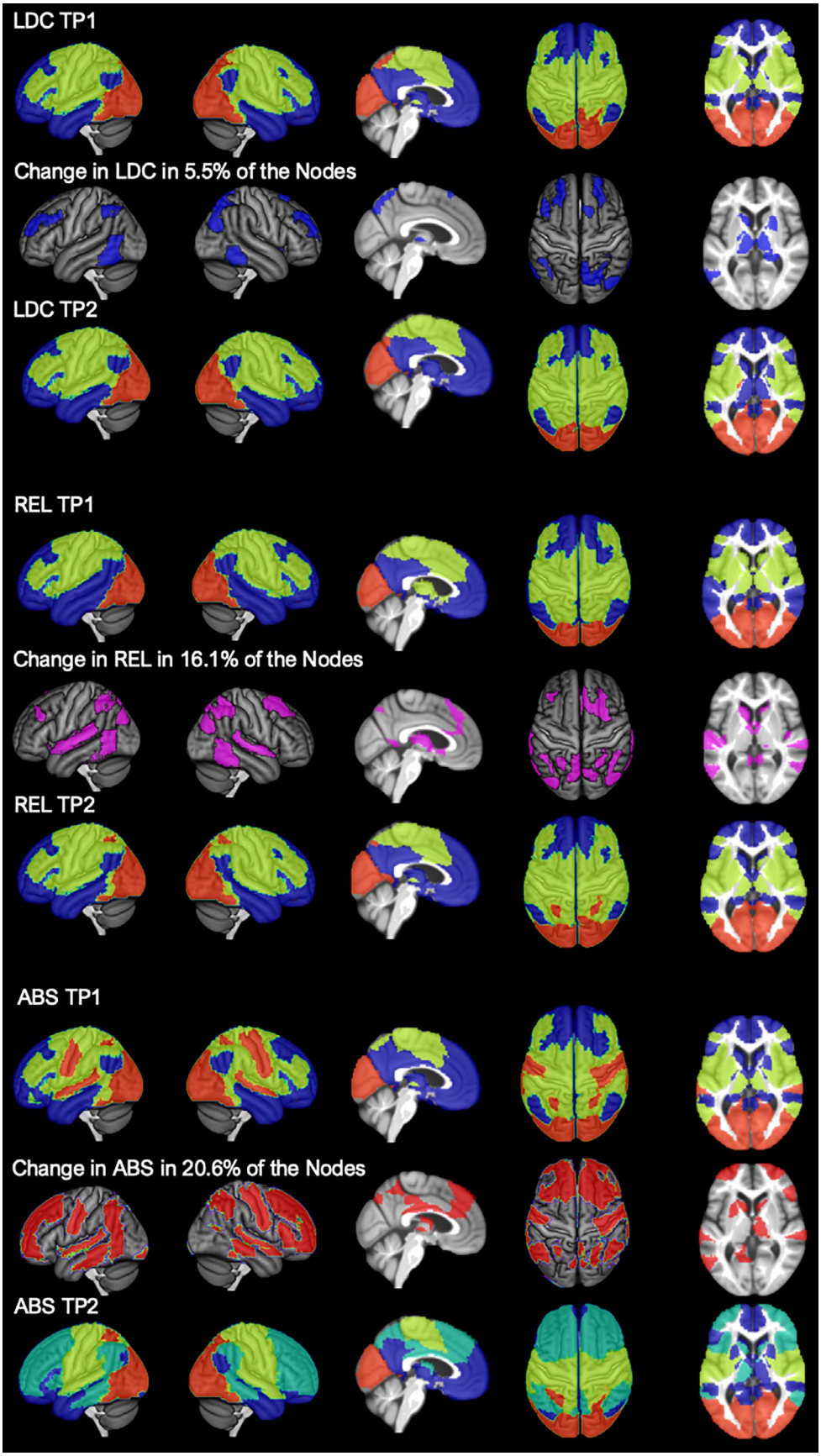

FIGURE 1 Group- and timepoint specific community configurations and within-group change in percent: We found a 3-community configuration for all three groups at timepoint 1 and for the controls and relapsers at timepoint 2. The abstainers underwent a reconfiguration in the three months interval and presented with a 4-community configuration at timepoint 2. ABS = abstainers; LDC, (light drinking) controls; REL = relapsers, TP = timepoint. The color code is as follows: dark blue = community 1; light green = community 2/2b; red = community 3; dark green = community 2a

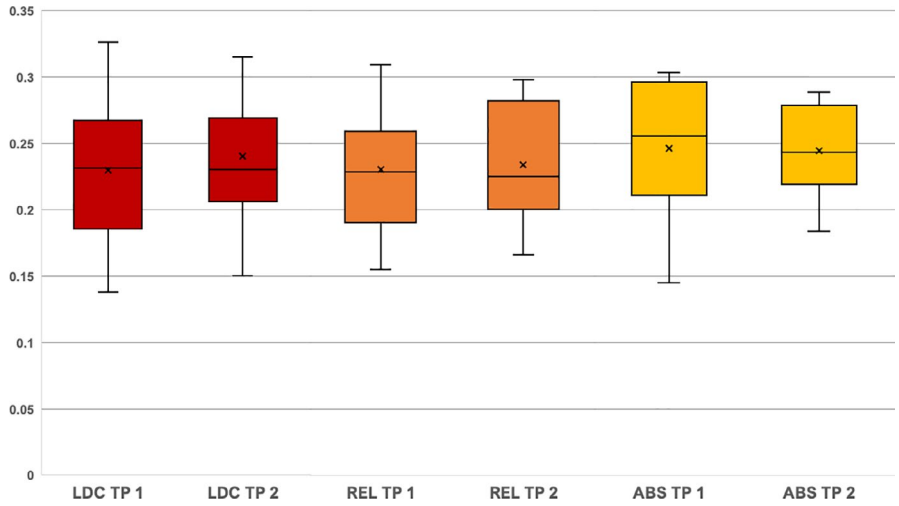

FIGURE 2 Group- and timepoint-specific maximum Q values. The Q values are shown on the *y* axis, the three groups (red = controls (LDC); orange = relapsers (REL); yellow = abstainers (ABS)) and the timepoints (TP) are shown on the *x* axis. The boxplots show the median value as a line and the mean value as a cross. The body represents the interquartile distance and the whiskers the lowest and highest Q value. At timepoint 1, controls and relapsers had approximately the same Q values (controls versus relapsers $p = .94$). Abstainers had higher Q values than the other two groups but not significantly higher (abstainers versus controls $p = .27$; abstainers versus relapsers $p = .24$). At timepoint 2, relapsers had minimally lower Q values than controls (controls versus relapsers $p = .72$). Abstainers had again the highest Q values but not significantly higher (abstainers versus controls $p = .59$; abstainers versus relapsers $p = .53$) and not as high as at timepoint 1

TABLE 2 Results of the permutation statistics–the community configurations are similar but still significantly specific for each group at each timepoint

	TP1			
	Community 1	**Community 2**	**Community 3**	
REL versus LDC	0% ($p < .0002$)	0.02% ($p = .0006$)	0.02% ($p < .0006$)	
ABS versus LDC	0% ($p < .0002$)	0.04% ($p = .0012$)	0% ($p < .0002$)	
REL versus ABS	0% ($p < .0002$)	0% ($p < .0002$)	2.96% (ns)	
ABS versus REL	0% ($p < .0002$)	0.42% ($p = .0126$)	0.06% ($p = .0018$)	
	TP 2			
	Community 1	**Community 2**	**Community 3**	
REL versus LDC	0.52% ($p = .0156$)	0% ($p < .0002$)	5.2% (ns)	
REL versus ABS	3.36% (ns)	0.02% ($p = .0006$)	0.82% ($p = .0246$)	
	Core-Community 1	**Community 2a**	**Community 2b**	**Community 3**
ABS versus LDC	0% ($p < .0002$)	0% ($p < .0002$)	0% ($p < .0002$)	0% ($p < .0002$)
ABS versus REL	0% ($p < .0002$)	0% ($p < .0002$)	0.12% ($p = .0048$)	0.92% ($p = .0368$)

Note: The first column of the table specifies the two groups whose data were permutated, e.g, REL versus LDC at TP1 means that we tested how probable it is that the relapser-specific community configuration at timepoint 1 could have been observed by chance in the controls at timepoint 1. The first number is the frequency in percent that the community configuration was observed across the 5,000 iterations, the corresponding p value (Bonferroni corrected) is given in brackets. For example, the exact node combination of community 2 in relapsers versus controls at timepoint 1 was only detected in 0.02% of the 5,000 iterations. A percentage that small corresponds to a p value = 0.0006 thereby community 2 is significantly specific for relapsers at timepoint 1.

Abbreviations: ABS, abstainers; LDC, light drinking controls; REL, relapsers; TP, timepoint.

4.5 | Specific features of the four-community configuration of the abstainers at follow-up

Figures S1e, S1f in the supplement indicate that the allocation of one of the DMN's subsystems, the dmPFC subsystem, to community 2a could be a specific feature of abstainers at follow-up. Using permutation statistics, we confirmed that the grouping of the dmPFC subsystem with the ECN, SN, and DAN into a separate community 2a was specific for abstainers. The probability to observe this abstainer-specific configuration by chance in controls was 0.04% ($p = .0004$) and in relapsers 0.02% ($p = .0002$).

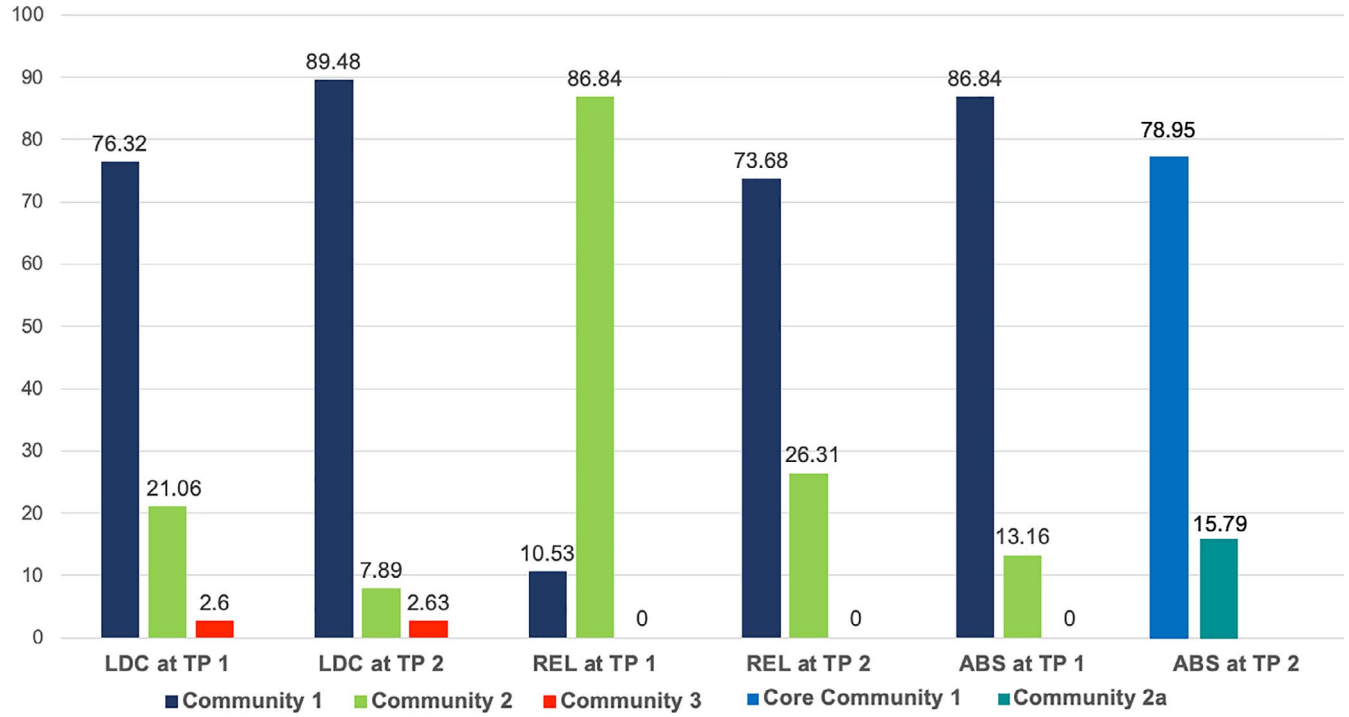

FIGURE 3 Percentage of basal ganglia and thalamus nodes allocated to one of the three communities in the controls (LDC, left), relapsers (REL, middle), and abstainers (ABS, right) by timepoint (TP). Most prominent is the different community allocation of the relapsers at timepoint 1 to that of the controls and abstainers at timepoint 1. Most of the controls' and abstainers' basal ganglia and thalamus nodes were allocated to community 1 at timepoint 1 (dark blue bars). In contrast, the relapsers' basal ganglia and thalamus nodes were more highly interconnected with community 2 nodes (light green bars). At timepoint 2, after the relapsers had started consuming alcohol again, the relapsers' community allocation resembled that of the controls

As a direct result of the allocation of the dmPFC subsystem to the abstainer-specific community 2a, the abstainers also showed a special allocation of the eBRS regions at follow-up (Figure 4). Whereas 87%–94% of the eBRS nodes in controls and relapsers were allocated to community 1 and only 6%–13% to community 2 (Table 3), 19% of the eBRS nodes in abstainers was allocated to the new community 2a and only 79% of the nodes to the new, reduced community 1. These eBRS region allocations were unique for the abstainers' four-community configuration at follow-up, and permutation testing showed that they were uniquely specific for the abstainers and could only have been found with a 0.1% chance (p =.001) in one of the other two groups.

4.6 | Results for the "global integration coefficient" (GIC): Degree of integration between communities

We did not observe GIC differences between controls and abstainers at baseline (Table 4 and Figure 5). In both groups, community 1 was characterized by a negative average GIC, indicating segregation from the other two communities. In contrast, the relapsers at baseline showed a positive GIC value for community 1. Subsequent Wilcoxon Sum Rank tests confirmed that the relapsers' community 1 at baseline was significantly over-integrated in the between-community-interaction compared to both controls and abstainers. Additionally, community 2 showed a negative GIC value in the relapsers at baseline but not in the controls and abstainers, indicating segregation of community 2 from the between-community-interaction in relapsers. The follow-up Wilcoxon Sum Rank tests confirmed that community 2 was de-connected in relapsers compared to controls and abstainers. The group-differences in between-community integration observed for relapsers at baseline were no longer present at follow-up when relapsers showed the same GIC pattern as the controls (negative GIC value for community 1 and positive GIC value for community 2). Abstainers showed similar between-community integration patterns at both timepoints. The abstainer-specific reduced communities 1 and 2a were both characterized by negative GIC values, indicating segregation from their global between-community interactions. Due to the abstainers' different community configurations at follow-up, it was not possible to compare them directly to the controls or relapsers.

5 | DISCUSSION

The aim of this study was to test if modularity (Q), recently suggested as a biomarker for brain plasticity (Gallen

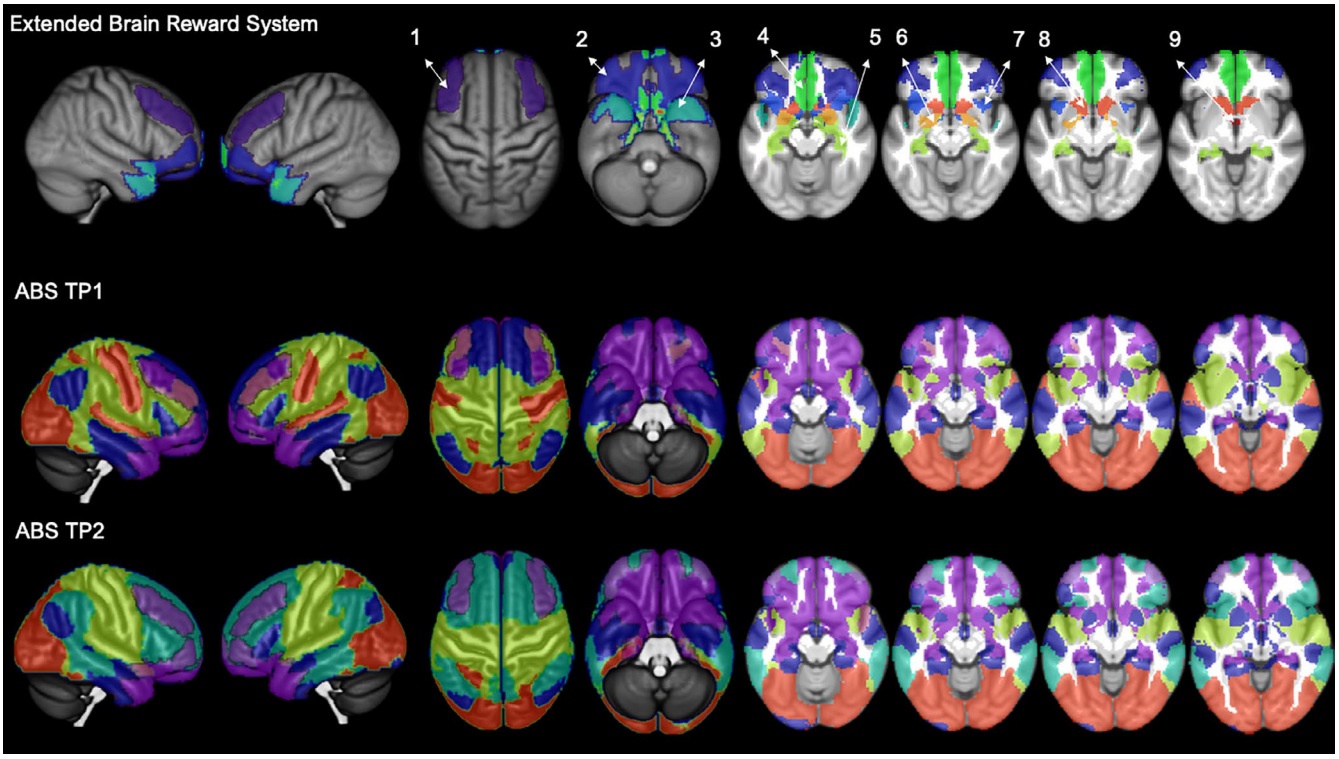

FIGURE 4 Abstainers (ABS) show a different allocation of the extended brain reward system (eBRS) at timepoint (TP) 2 as a result of the re-configuration. The top row shows the 9 regions of the eBRS with 1 = dorsolateral prefrontal cortex (PFC), 2 = orbital PFC; 3 = temporal pole; 4 = ventromedial PFC; 5 = hippocampus; 6 = amygdala; 7 = anterior insula; 8 = nucleus accumbens, 9 = anterior thalamus. The other rows show the abstainers' 3-community configuration at timepoint 1 (middle), and the 4-community configuration at timepoint 2 (bottom). At timepoint 1, the dorsolateral prefrontal eBRS region was allocated to community 1 and community 2; at timepoint 2, the dorsolateral prefrontal region was allocated to the new community 2a that we showed to be significantly specific to the abstainers at that timepoint. Brain regions belonging to the eBRS are highlighted in transparent violet to allow a better mapping of the eBRS region to the community structure

TABLE 3 Community allocation of the 62 nodes constituting the extended brain reward system (eBRS) in percent

	Community 1	Community 2	Core Community 1	Community 2a
LDC at TP1	93.55 (58)	6.45 (4)	—	—
LDC at TP2	90.32 (56)	9.68 (6)	—	—
REL at TP1	87.09 (54)	12.91 (8)	—	—
REL at TP2	93.55 (58)	6.45 (4)	—	—
ABS at TP1	93.55(58)	6.45 (4)	—	—
ABS at TP2	—	—	79.03 (49)	19.35 (12)

Note: The number of the total 62 eBRS nodes within each of the different communities is listed in brackets.
Abbreviations: ABS, abstainers; LDC, light drinking controls; REL, relapsers; TP, timepoint.

& D'Esposito, 2019), and the corresponding group-specific community configurations can help explain features of the intrinsic brain organization in individuals with AUD that are associated with sustained abstinence or relapse after treatment. Such markers may have clinical utility in predicting relapse in treatment seekers.

We found that abstainers at the 1-month baseline and 3 months later had (non-significantly) higher Q values than controls and relapsers, indicating a higher potential for brain plasticity. Controls and relapsers, who had similar Q values at both timepoints, had approximately the same potential for neuroplasticity. All three groups had a similar three-community configuration at baseline, sharing the community allocation of 80%–90% of the nodes. Despite the visual resemblance, the group-specific community configurations were unique, since none of them could have been found by chance in any of the other two groups. The most prominent difference between the groups across time resulted from a

TABLE 4 Global Integration Coefficient (GIC) median values and results of the Wilcoxon Rank Sum tests for group differences by community and timepoint

Timepoint 1					
		Community 1	**Community 2**	**Community 3**	
GIC values	LDC	−0.0484 (0.053)	0.0589 (0.095)	0.1013 (0.087)	
	REL	0.0167 (0.067)	−0.0132 (0.049)	0.1285 (0.062)	
	ABS	−0.0714 (0.083)	0.0785 (0.172)	0.1269 (0.124)	
Wilcoxon Rank Sum	LDC versus REL	$p < .0009$ ($Z = 4.16$; effect size $r = 0.58$)	$p < .0009$ ($Z = -4.2136$; effect size $r = -0.58$)	ns	
	LDC versus ABS	ns	ns	ns	
	REL versus ABS	$p = .0036$ ($Z = 3.5136$; effect size $r = 0.60$)	$p = .0027$ ($Z = -3.5857$; effect size $r = -0.61$)		
Timepoint 2					
		Community 1	**Community 2**	**Community 3**	
GIC values	LDC	−0.0538 (0.059)	0.0724 (0.086)	0.1199 (0.059)	
	REL	−0.0303 (0.060)	0.0317 (0.113)	0.1036 (0.085)	
Wilcoxon Rank Sum	LDC versus REL	ns	ns	ns	
		Core Community 1	**Community 2a**	**Community 2b**	**Community 3**
GIC values	ABS	0.0048 (0.076)	−0.0333 (0.041)	0.081 (0.093)	0.084 (0.067)

Note: GIC values listed as median with interquartile distance in brackets. The *p*-values are listed after Bonferroni corrected for multiple comparisons. Only the relapsers revealed significant group differences in the mean GIC values of the communities at timepoint 1, no significant differences between relapsers and controls at timepoint 2.

Abbreviations: ABS, abstainers; LDC, light drinking controls; REL, relapsers.

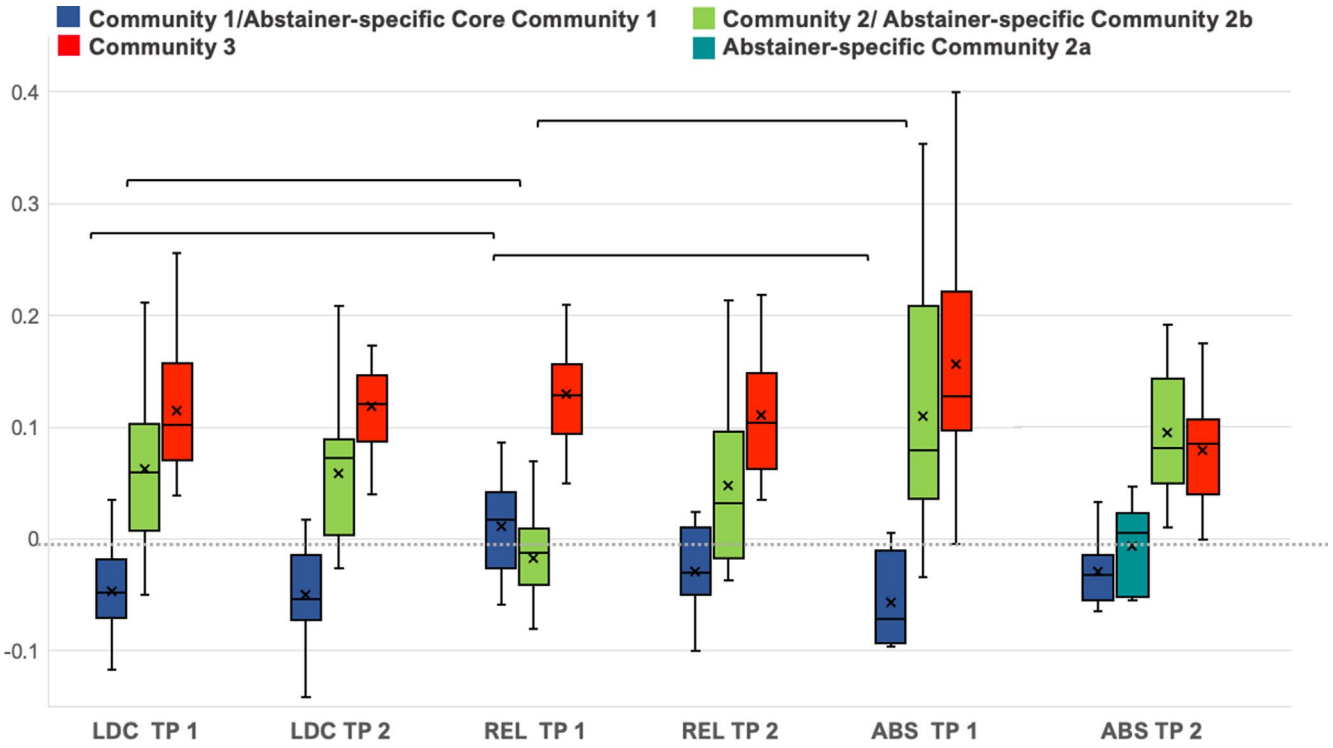

FIGURE 5 Global Integration Coefficient (GIC) by group and timepoint for the different communities. The solid line in each box indicates the group median value, the cross indicates the group mean value, the whiskers indicate the lowest and the highest GIC values, the brackets indicate significant group differences in GIC. The community specific GIC of relapsers (REL, middle) at timepoint (TP) 1 significantly differs from that of controls (LDC, left) and abstainers (ABS, right) at timepoint 1. Community 1 of the abstainers and controls showed negative mean GIC values indicating segregation from the other two communities in these two groups, the relapsers' community 1 was characterized by global integration with the other two communities as indicated by positive mean GIC values of that community. In contrast, while community 2 showed global integration in the controls and abstainers, the same community was characterized by segregation in the relapsers at timepoint 1. The group differences in global integration of the communities between relapsers and the other two groups were significant at timepoint 1 but not anymore at timepoint 2

re-configuration in the abstainers between baseline and follow-up. Whereas at follow-up, controls and relapsers presented with almost the same three-module-configuration as at baseline, abstainers showed an additional fourth module, reducing the shared community allocation to 60%–90% of the nodes.

Relapsers also underwent some degree of re-configuration that manifested itself in a change in the allocation of caudate and thalamus nodes from community 2 at baseline to community 1 at follow-up. In controls and abstainers, those nodes were primarily allocated to community 1 at both timepoints. This indicates that these regions interacted with different intrinsic connectivity networks (ICN) in relapsers than in controls and abstainers 1 month into abstinence. At follow-up, after relapsers had started consuming alcohol again, their thalamus and caudate nodes were also allocated to community 1, just as in controls and abstainers. Finally, relapsers revealed distinct differences in how the three communities globally interacted with each other at baseline but not anymore 3 months later. In the following sections, we will discuss the most important findings and their interpretations in more detail.

5.1 | Community re-configuration in the abstainers from baseline to follow-up

We found a similar three-community configuration in all three groups at baseline (DMN and limbic network allocated to community 1; ECN, DAN, SN, and SMN allocated to community 2; VIS constituting community 3). At follow-up, controls and relapsers still presented with a three-community configuration, whereas abstainers revealed a four-community configuration: the dmPFC subsystem was now separated from the core DMN and merged with the ECN, SN and DAN into a new community 2a, while the SMN became a new independent community 2b.

The DMN consists of a group of distinct brain regions that generally show higher activity when a person is not actively engaging with the external world but rather focusing on an internal flow of thoughts or mental images. In contrast to the view that the DMN always has the highest intrinsic activity at rest (Fox et al., 2006), studies have recently demonstrated that intrinsic activity, measured by functional connectivity within and between intrinsic networks, fluctuates and that the spatial extent of the networks

varies over time. For example, Chen et al. (2018) showed that the brain dynamically traverses two distinct activity patterns during unconstrained rest: 60% of the time the brain shows a pattern that closely resembles the DMN, but for 40% of the time the brain shows a pattern very similar to that of a task-positive network. This network shows high levels of activity during active goal-driven behavior (Fox et al., 2006), and it is composed of ECN, DAN, ventral attention network, SN, motor network, auditory network, VIS, as well as a part of the DMN (Chen et al., 2018). Di and Biswal (2015) compared states of low versus high intrinsic activity in the DMN, SN, and motor networks. They found that phases of high DMN activity were characterized by decreased connectivity between DMN regions but increased connectivity between regions belonging to the fronto-parietal control network. In contrast, during phases of high SN activity, DMN and fronto-parietal control network showed higher inter-network connectivity.

Based on these studies, the re-configuration found in abstainers at follow-up indicates that they were in a more controlled state of deliberate mind-wandering than controls and relapsers. Deliberate is different from spontaneous mind-wandering insofar as the latter happens involuntarily and is experienced as interfering with one's intentions, whereas deliberate mind-wandering is experienced as a voluntary and controlled train of thought in accordance with one's intentions (Golchert et al., 2017). As such, deliberate mind-wandering requires integration of DMN and ECN (Smallwood et al., 2012; Golchert et al., 2017) in order to exert a top-down control to shield the abstract flow of thoughts from external disturbances. Strong and stable coupling of ECN and DMN (as reflected in a subsystem of DMN interacting most of the time and more intensely with ECN than with its own core network), is exactly what the abstainers exhibited at follow-up.

Abstainers at follow-up showed an additional feature shown specifically to deliberate mind-wandering: the internal thought process has to be shielded from irrelevant input from the outside by a temporary decoupling of the brain regions processing perceptual information (Smallwood et al., 2012). Evidence of such decoupling can be seen in our finding that communities 1 and 2a in abstainers showed an altered global between-community integration at follow-up: While community 2 had shown between-community integration with community 3 at baseline (i.e., both communities had positive GIC values), community 1 and the new community 2a were both segregated (i.e., they had negative GIC values) from communities 2b 3 at follow-up.

The re-configuration of the community structure in the abstainers at follow-up had also consequences for the integration of the eBRS within the community structure. At baseline, all three groups showed an almost identical allocation (i.e., >87% of the eBRS nodes were allocated to community 1). At follow-up, the dorsolateral prefrontal part of the eBRS in the abstainers was entirely re-allocated to the new fourth community composed of the dmPFC subsystem, the ECN, DAN, and SN. We suggest that the re-allocation of the eBRS might be an indicator of the abstainers' executive control over the eBRS being so intense/strong during the first months into sobriety that it re-shaped the intrinsic organization of their brains, while they successfully maintained sobriety for 4 months.

5.2 | Caudate and thalamus show different resting-state network interactions in relapsers than in abstainers and controls

Alves et al. (2019), using an advanced coregistration based on functional alignment, recently showed that thalamus and basal ganglia, particularly caudate nucleus, belong to the DMN. Their subsequent tractography analyses not just supported these functional findings but also revealed a central role of the thalamus within the DMN for information integration and resilience. In line with these findings, controls and abstainers of our study showed a stable allocation of the thalamus and the basal ganglia to the DMN (community 1), at both timepoints. In contrast, in relapsers at baseline, most thalamic nodes were assigned to community 2 consisting of the ECN, DAN, SN, and SMN. This suggests a higher interconnectedness of the thalamus and the caudate nucleus with these four ICNs in relapsers than with the DMN. Taken together, we interpret the altered allocation of thalamus and caudate nucleus in relapsers at baseline as an indicator of functional de-differentiation.

5.3 | Different global between-community integrations in the relapsers at baseline: An early indicator of future relapse?

Abstainers and controls showed the same global-between-community integration pattern at baseline: community 1 was segregated or decoupled (negative GIC values) from the global between-community crosstalk, while communities 2 and 3 (positive GIC values) interacted with each other. In contrast, relapsers showed the reverse pattern: community 1 (usually segregated from primary ICNs like the visual, auditory or motor network) was coupled with community 3, while community 2 (containing three important ICNs involved in top-down control: the ECN, SN, and DAN) was decoupled from the other two communities. Thus, we postulate that in the abstainers and controls, the intrinsic brain network architecture allowed exercising top-down control with minimal reconfiguration and energetic costs whenever external events demanded so, however, the relapsers would need to substantially reconfigure their intrinsic brain configuration in order

to exercise effective top-down control (Bell et al., 2014). Additionally, the relapsers' functional brain organization would require more energy-demanding effort to maintain top-down control during the first month of sobriety, when top-down control is essential for maintaining abstinence.

6 | LIMITATIONS

The relatively small number of abstainers at both timepoints and the unbalanced group sizes are certainly the most important limitations of our study. The main reason for the abstainers' small sample size is the notoriously high relapse rate in AUD (40%–60%) within the first 6 months after treatment in combination with the rigorous exclusion of data sets with motion artifacts and other noise to guarantee that our findings were based on data of highest quality. Sample size and the VA as primary recruitment source were also reasons for our inability to investigate potential sex differences.

Furthermore, these are cross-sectional analyses of AUD patients 1 month into treatment and 3 months later. We found characteristic differences in intrinsic network organization early in treatment with the potential to predict future relapsers in a different cohort. However, we do not know whether the intrinsic network organization of abstainers and relapsers already differed at the start of their treatment (i.e., before baseline) or whether the differences resulted from different neuroplastic alterations during the first month of sobriety. We also are unable to ascertain whether these differences in the intrinsic network organization observed in abstainers are just transient snap-shots typical for an early timepoint in a lifelong effort to stay sober, whether their intrinsic network organization will become more similar to that of controls over time, or whether the distinct four-community configuration in abstainers is just the brain configuration necessary to stay sober for the rest of their lives. Well-timed longitudinal assessments could address these limitations in the future.

7 | CONCLUSIONS

Relapsers as early as 1 month into treatment have indications of a maladaptive community configuration. The community containing the DMN, an ICN that is usually characterized by de-coupling from primary ICNs like the auditory or visual networks, was over-integrated with the visual community, while the community containing the ICNs important for top-down control was de-connected from the between-community integration. This community configuration is unsuitable for situations in which the ability to initiate active top-down control over urges to drink is essential. An unexpected study finding was that successful recovery from AUD, as seen in abstainers, is not associated with re-gaining the intrinsic brain organization typical for controls, but with a re-configuration resulting in a functional brain organization significantly different from that of controls. A distinctive feature of the abstainers' re-configured intrinsic brain organization was the stronger functional coupling of a DMN subsystem, the dmPFC, and parts of the eBRS with ICNs subserving top-down control and attention so that these networks formed an additional separate community in abstainers.

ACKNOWLEDGMENTS

This work was supported by NIH AA010788, DA039903, and DoD W81XWH-15-2-0020 (all to DJM) and by San Francisco VA Medical Center resources. The research was administered by the Northern California Institute for Research and Education. The funding and administrative agencies had no role in the design of the study, collection, and analysis of data or the decision to publish. We extend our appreciation to all who volunteered for this research. For critical help with participant recruitment, we thank the substance abuse treatment personnel at the San Francisco VA as well as Dr. David Pating and his team at Kaiser Permanente San Francisco. We also wish to thank Thomas Schmidt, Randi Brown, and Rachel Gonzalez for participant recruitment and assessment as well as Alen Tersakyan for MR data acquisition.

CONFLICT OF INTEREST

The authors declare no conflict of interest.

AUTHOR CONTRIBUTIONS

DJM conceptualization, funding acquisition, resources, supervision, writing (review and editing); AMM conceptualization, formal analysis, methodology, visualization, writing (original draft preparation, reviewing, and editing).

Peer Review

The peer review history for this article is available at https://publons.com/publon/10.1111/ejn.15161.

DATA AVAILABILITY STATEMENT

Restrictions apply to the data sets: the data sets for this manuscript are not publicly available because they were created as part of Veteran's Administration-approved research. Requests to access the data sets should be directed to the senior author).

ORCID

Angela M. Muller https://orcid.org/0000-0002-9866-2285
Dieter J. Meyerhoff https://orcid.org/0000-0002-2433-7826

REFERENCES

Alves, P. N., Foulon, C., Karolis, V., Bzdok, D., Margulies, D. S., Volle, E., & Thiebaut de Schotten, M. (2019). An improved neuroanatomical model of the default-mode network reconciles previous

neuroimaging and neuropathological findings. *Communications Biology*, *2*, 370. https://doi.org/10.1038/s42003-019-0611-3

Andrews-Hanna, J. R., Reidler, J. S., Sepulcre, J., Poulin, R., & Buckner, R. L. (2010). Functional-anatomic fractionation of the brain's default network. *Neuron*, *65*(4), 550–562. https://doi.org/10.1016/j.neuron.2010.02.005

Arnemann, K. L., Chen, A. J., Novakovic-Agopian, T., Gratton, C., Nomura, E. M., & D'Esposito, M. (2015). Functional brain network modularity predicts response to cognitive training after brain injury. *Neurology*, *84*(15), 1568–1574. https://doi.org/10.1212/WNL.0000000000001476

Ashburner, J. (2007). A fast diffeomorphic image registration algorithm. *NeuroImage*, *38*(1), 95–113. https://doi.org/10.1016/j.neuroimage.2007.07.007

Baniqued, P. L., Gallen, C. L., Kranz, M. B., Kramer, A. F., & D'Esposito, M. (2019). Brain network modularity predicts cognitive training-related gains in young adults. *Neuropsychologia*, *131*, 205–215. https://doi.org/10.1016/j.neuropsychologia.2019.05.021

Baniqued, P. L., Gallen, C. L., Voss, M. W., Burzynska, A. Z., Wong, C. N., Cooke, G. E., Duffy, K., Fanning, J., Ehlers, D. K., Salerno, E. A., Aguiñaga, S., McAuley, E., Kramer, A. F., & D'Esposito, M. (2018). Brain network modularity predicts exercise-related executive function gains in older adults. *Frontiers in Aging Neuroscience*, *9*, 426. https://doi.org/10.3389/fnagi.2017.00426

Bassett, D. S., Bullmore, E., Verchinski, B. A., Mattay, V. S., Weinberger, D. R., & Meyer-Lindenberg, A. (2008). Hierarchical organization of human cortical networks in health and schizophrenia. *The Journal of Neuroscience: The Official Journal of the Society for Neuroscience*, *28*(37), 9239–9248. https://doi.org/10.1523/JNEUROSCI.1929-08.2008

Beck, A. T., Ward, C. H., Mendelson, M., Mock, J., & Erbaugh, J. (1961). An inventory for measuring depression. *Archives of General Psychiatry*, *4*, 561–571. https://doi.org/10.1001/archpsyc.1961.01710120031004

Behzadi, Y., Restom, K., Liau, J., & Liu, T. T. (2007). A component based noise correction method (CompCor) for BOLD and perfusion based fMRI. *NeuroImage*, *37*(1), 90–101. https://doi.org/10.1016/j.neuroimage.2007.04.042

Bell, R. P., Garavan, H., & Foxe, J. J. (2014). Neural correlates of craving and impulsivity in abstinent former cocaine users: Towards biomarkers of relapse risk. *Neuropharmacology*, *85*, 461–470. https://doi.org/10.1016/j.neuropharm.2014.05.011

Betzel, R. F., & Bassett, D. S. (2017). Multi-scale brain networks. *NeuroImage*, *160*, 73–83. https://doi.org/10.1016/j.neuroimage.2016.11.006

Blondel, V. D., Guillaume, J. L., Lambiotte, R., & Lefebvre, E. (2008). Fast unfolding of communities in large networks. *Journal of Statistical Mechanics: Theory and Experiment*, *2008*, P10008. https://doi.org/10.1088/1742-5468/2008/10/P10008

Brooks, S. J., Mackenzie-Phelan, R., Tully, J., & Schiöth, H. B. (2020). Review of the neural processes of working memory training: Controlling the impulse to throw the baby out with the bathwater. *Frontiers in Psychiatry*, *11*, 512761. https://doi.org/10.3389/fpsyt.2020.512761

Bullmore, E., & Sporns, O. (2012). The economy of brain network organization. *Nature Reviews. Neuroscience*, *13*(5), 336–349. https://doi.org/10.1038/nrn3214

Chen, R. H., Ito, T., Kulkarni, K. R., & Cole, M. W. (2018). The human brain traverses a common activation-pattern state space across task and rest. *Brain Connectivity*, *8*(7), 429–443. https://doi.org/10.1089/brain.2018.0586

Cohen, J. R., & D'Esposito, M. (2016). The segregation and integration of distinct brain networks and their relationship to cognition. *The Journal of Neuroscience: The Official Journal of the Society for Neuroscience*, *36*(48), 12083–12094. https://doi.org/10.1523/JNEUROSCI.2965-15.2016

Di, X., & Biswal, B. B. (2015). Characterizations of resting-state modulatory interactions in the human brain. *Journal of Neurophysiology*, *114*(5), 2785–2796. https://doi.org/10.1152/jn.00893.2014

Doucet, G. E., Lee, W. H., & Frangou, S. (2019). Evaluation of the spatial variability in the major resting-state networks across human brain functional atlases. *Human Brain Mapping*, *40*(15), 4577–4587. https://doi.org/10.1002/hbm.24722

Durazzo, T. C., Tosun, D., Buckley, S., Gazdzinski, S., Mon, A., Fryer, S. L., & Meyerhoff, D. J. (2011). Cortical thickness, surface area, and volume of the brain reward system in alcohol dependence: Relationships to relapse and extended abstinence. *Alcoholism, Clinical and Experimental Research*, *35*(6), 1187–1200. https://doi.org/10.1111/j.1530-0277.2011.01452.x

Fox, M. D., Snyder, A. Z., Zacks, J. M., & Raichle, M. E. (2006). Coherent spontaneous activity accounts for trial-to-trial variability in human evoked brain responses. *Nature Neuroscience*, *9*(1), 23–25. https://doi.org/10.1038/nn1616

Gallen, C. L., Baniqued, P. L., Chapman, S. B., Aslan, S., Keebler, M., Didehbani, N., & D'Esposito, M. (2016). Modular brain network organization predicts response to cognitive training in older adults. *PLoS One*, *11*(12), e0169015. https://doi.org/10.1371/journal.pone.0169015

Gallen, C. L., & D'Esposito, M. (2019). Brain modularity: A biomarker of intervention-related plasticity. *Trends in Cognitive Sciences*, *23*(4), 293–304. https://doi.org/10.1016/j.tics.2019.01.014

Girvan, M., & Newman, M. E. (2002). Community structure in social and biological networks. *Proceedings of the National Academy of Sciences*, *99*(12), 7821–7826. https://doi.org/10.1073/pnas.122653799

Guimerà, R., & Amaral, L. A. Cartography of complex networks: modules and universal roles. *Journal of Statistical Mechanics: Theory and Experiment*, *2005*(02), P02001–https://doi.org/10.1088/1742-5468/2005/02/P02001

Hallquist, M. N., & Hillary, F. G. (2018). Graph theory approaches to functional network organization in brain disorders: A critique for a brave new small-world. *Network Neuroscience (Cambridge, Mass.)*, *3*(1), 1–26. https://doi.org/10.1162/netn_a_00054

Heatherton, T. F., Kozlowski, L. T., Frecker, R. C., & Fagerström, K. O. (1991). The fagerström test for nicotine dependence: A revision of the fagerström tolerance questionnaire. *British Journal of Addiction*, *86*(9), 1119–1127.

Kirshenbaum, A. P., Olsen, D. M., & Bickel, W. K. (2009). A quantitative review of the ubiquitous relapse curve. *Journal of Substance Abuse Treatment*, *36*(1), 8–17. https://doi.org/10.1016/j.jsat.2008.04.001

Lancichinetti, A., & Fortunato, S. (2012). Consensus clustering in complex networks. *Scientific Reports*, *2*, 336. https://doi.org/10.1038/srep00336

Makris, N., Oscar-Berman, M., Jaffin, S. K., Hodge, S. M., Kennedy, D. N., Caviness, V. S., Marinkovic, K., Breiter, H. C., Gasic, G. P., & Harris, G. J. (2008). Decreased volume of the brain reward system in alcoholism. *Biological Psychiatry*, *64*(3), 192–202. https://doi.org/10.1016/j.biopsych.2008.01.018

Meyerhoff, D. J., & Durazzo, T. C. (2020). Modelling neurocognitive and neurobiological recovery in addiction. In A. Verdejo-Garcia (Ed.), *Cognition and addiction. A researcher's guide from mechanisms toward interventions* (1st ed., pp. 379–386). Cambridge, MA: Academic Press.

Patton, J. H., Stanford, M. S., & Barratt, E. S. (1995). Factor structure of the Barratt impulsiveness scale. *Journal of Clinical Psychology*, *51*(6), 768–774.

Rubinov, M., & Sporns, O. (2010). Complex network measures of brain connectivity: Uses and interpretations. *NeuroImage*, *52*(3), 1059–1069. https://doi.org/10.1016/j.neuroimage.2009.10.003

Rubinov, M., & Sporns, O. (2011). Weight-conserving characterization of complex functional brain networks. *NeuroImage*, *56*(4), 2068–2079. https://doi.org/10.1016/j.neuroimage.2011.03.069

Santarnecchi, E., Galli, G., Polizzotto, N. R., Rossi, A., & Rossi, S. (2014). Efficiency of weak brain connections support general cognitive functioning. *Human Brain Mapping*, *35*(9), 4566–4582. https://doi.org/10.1002/hbm.22495

Saunders, J. B., Aasland, O. G., Babor, T. F., de la Fuente, J. R., & Grant, M. (1993). Development of the Alcohol Use Disorders Identification Test (AUDIT): WHO collaborative project on early detection of persons with harmful alcohol consumption II. *Addiction*, *88*, 791–804. https://doi.org/10.1111/j.1360-0443.1993.tb02093.x

Smallwood, J., Brown, K., Baird, B., & Schooler, J. W. (2012). Cooperation between the default mode network and the frontal-parietal network in the production of an internal train of thought. *Brain Research*, *1428*, 60–70. https://doi.org/10.1016/j.brainres.2011.03.072

Spielberger, C. D. (1983). *Manual for the State-Trait Anxiety Inventory for Adults (STAI-AD)*. Consulting Psychologists Press.

Sporns, O., & Betzel, R. F. (2016). Modular brain networks. *Annual Review of Psychology*, *67*, 613–640. https://doi.org/10.1146/annurev-psych-122414-033634

van den Heuvel, M. P., de Lange, S. C., Zalesky, A., Seguin, C., Yeo, B., & Schmidt, R. (2017). Proportional thresholding in resting-state fMRI functional connectivity networks and consequences for patient-control connectome studies: Issues and recommendations. *NeuroImage*, *152*, 437–449. https://doi.org/10.1016/j.neuroimage.2017.02.005

Zalesky, A., Fornito, A., Cocchi, L., Gollo, L. L., & Breakspear, M. (2014). Time-resolved resting-state brain networks. *Proceedings of the National Academy of Sciences of the United States of America*, *111*(28), 10341–10346. https://doi.org/10.1073/pnas.1400181111

SUPPORTING INFORMATION

Additional supporting information may be found online in the Supporting Information section.

How to cite this article: Muller AM, Meyerhoff DJ. Maladaptive brain organization at 1 month into abstinence as an indicator for future relapse in patients with alcohol use disorder. *Eur J Neurosci*. 2021;53:2923–2938. https://doi.org/10.1111/ejn.15161